RADIATION LABORATORY

UCRL-1109
Unclassified Physics

Phys Rev 1951

UNIVERSITY OF CALIFORNIA

Radiation Laboratory

Contract No. W-7405-eng-48

Experiments on Proton-Proton Scattering from 120 to 345 Mev

O. Chamberlain, E. Segrè and C. Wiegand

February 1951

Same as Phys. Rev. 83, 923 (1951)

Berkeley, California

Experiments on Proton-Proton Scattering from 120 to 345 Mev

O. Chamberlain, E. Segrè and C. Wiegand

Radiation Laboratory, Department of Physics
University of California, Berkeley, California

February 1951

ABSTRACT

The differential scattering cross section for elastic collisions of 345 Mev protons with protons has been measured in the angular range 11° to 90° (center of mass system). The same cross section has been measured over more limited ranges of angles at lower energies. The cross section (in the center of mass system) at 90° is remarkably independent of energy. The cross section at 345 Mev is very independent of angle, being close to 3.8×10^{-27} cm^2/steradian (center of mass system). The agreement with existing phenomenological theories based on static potentials is rather poor, especially in the case of scattering at small angles at 345 Mev.

Experiments on Proton-Proton Scattering from 120 to 345 Mev

O. Chamberlain, E. Segrè and C. Wiegand

Radiation Laboratory, Department of Physics
University of California, Berkeley, California

February, 1951

Introduction

The results of experimental investigations of n-p scattering have previously been reported and we have given preliminary reports on our study of p-p scattering.[1,2]

At the end of one preliminary report, we indicated some possible improvements in technique which we have now accomplished. In this paper we give our final results on the differential cross section of proton-proton scattering as a function of the angle of scattering and of the energy of the protons. The results of our preliminary paper are confirmed, but the present investigation extends the data to lower energies and increases the precision of the determinations. While these experiments were in progress, Oxley, Schamberger, and Towler[3] have investigated the p-p scattering at 240 Mev, and Birge[4] has done the same at 100 Mev. Their results overlap in part our own and agree with us in the common part.

A summary of the results is presented in Tables I, II, III and in Fig. 10.

---

[1] Hadley, Kelly, Leith, Segrè, Wiegand, and York, Phys. Rev. 75, 351 (1949); Kelly, Leith, Segrè, and Wiegand, Phys. Rev. 79, 96 (1950).

[2] O. Chamberlain and C. Wiegand, Phys. Rev. 79, 81 (1950); Chamberlain, Segrè, and Wiegand, Phys. Rev., in press.

[3] Oxley, Schamberger, and Towler, Bull. Amer. Phys. Soc. 26, 8 (1951).

[4] R. W. Birge, Phys. Rev. 80, 490 (1950).

Experimental

Our source of high energy protons is the external beam of the 184-inch Berkeley cyclotron. In this beam is placed a hydrogenous target; either polyethylene (CH_2) or liquid hydrogen. The protons scattered out of the beam (and out of the target) are counted either singly (method I) or else both the scattered and struck protons are detected simultaneously by two counters in coincidence (method II). In the latter case the two protons emerge from the target at about 90° from each other, a characteristic which helps very greatly in the separation of p-p scattering from other scattering processes. Both methods are aided by two developments: the invention by Leith of a method for obtaining a fairly long (25 microsecond) beam pulse time using deflection by multiple scattering within the cyclotron vacuum tank;[5] and the development of trans-stilbene crystal counters and associated equipment[6,7] with a resolving time for coincidences of about 4×10^{-8} sec.

A schematic diagram of the apparatus (method II) is presented in Fig. 1. The beam deflected from the cyclotron and collimated through the shielding walls impinges on the target T (a foil of polyethylene). The protons, scattered and recoil, are detected in the stilbene crystals A and B, each viewed by a 1P21 photomultiplier tube. A subtends the smaller solid angle Ω, and B is such that every proton through A sends its counterpart through B; as a matter of fact, B subtends a larger solid angle than would be necessary to satisfy the condition stated above in order to be safe from losses of coincidences due to multiple scattering effects and defects in alignment.

---

[5] C. E. Leith, Phys. Rev. 78, 89 (1950).

[6] Ginston, Hewlett, Jasberg, and Noe, Proc. I. R. E. 36, 956 (1948).

[7] C. Wiegand, Rev. Sci. Inst. 21, 975 (1950).

The beam is monitored by measuring the ionization produced in a shallow ionization chamber full of argon which has (in turn) been calibrated against a Faraday cup.

Let us call N the number of hydrogen atoms per cm^2 in the target measured in the direction of the incident beam, n the number of protons that crossed the target and H the number of coincidence counts between A and B due to hydrogen in the target. Let Φ be the angle between the line from the target to counter A and the direction of the primary beam. We have $\sigma(\Phi)$, the differential scattering cross section (laboratory system) given by

$$\sigma(\Phi) = H/(n\Omega N). \tag{1}$$

Passing to the center of mass system:

$$\sigma(\theta) = \frac{\left[1 + (E/2Mc^2) \sin^2 \Phi\right]^2}{1 + (E/2Mc^2)} \left(\frac{1}{4 \cos \Phi}\right) \sigma(\Phi), \tag{2}$$

$$\tan (\theta/2) = \left[1 + (E/2Mc^2)\right]^{1/2} \tan \Phi \tag{3}$$

where $\sigma(\theta)$ is the differential scattering cross section in the center of mass system, at angle θ from the beam in the center of mass system of coordinates, E is the kinetic energy of the incident protons (lab. system), Mc^2 is the proton rest energy.

We shall now describe our operations and the measurements of the single factors entering into Eq. (1).

Proton Beam

Fig. 2 gives a general plan of the cyclotron showing the path of the protons in the external beam. At large radii (about 81 inches) the proton orbits show large vertical oscillations and much of the internal beam strikes either of two graphite blocks placed above and below the normal beam plane. A few of the protons are deflected by multiple scattering in the graphite in such a way as to enter the magnetic shielding tube ("magnetic deflector")

through which the protons are led away from the main field of the cyclotron.

The collimator C is shown in more detail in Fig. 3. Its aperture can be changed from two inches to 1/4 inch; we used it in the range 1/2 to 1 inch. The axis of the collimator hole was adjusted to be parallel to the beam to within 0.001 radian. The central hole of the collimator could be preceded by cylindrical boxes full of lithium metal in order to reduce the energy of the emerging protons.

The homogeneity in energy of the emerging beam is very satisfactory as shown by the Bragg curve given in another article.[8] This is obtainable by putting 2 shallow ionization chambers in the beam between which is a variable copper absorber. The ratio of the current in the second chamber to that in the first chamber is plotted as a function of absorber thickness. The sharp peak at the end of the curve is an indication of the homogeneity in the energy of the beam.

The bending magnet in combination with the three collimating holes through which the beam must pass gives a momentum selection to about one percent. Evidence that few very low energy protons are generated in the collimator tube material is obtained from the coincidence counting method (as explained in connection with Fig. 8).

The current in the beam was measured in an ionization chamber of the type shown in Fig. 4, which was calibrated against a Faraday cup at the highest energy used (345 Mev). The Faraday cup, which is our primary standard for determination of the beam intensity, was built by Dr. V. Z. Peterson. It consists of a 6-inch by 6-inch cylindrical brass block, as shown in Fig. 4. Across the face of the Faraday cup is a thin foil (bias foil) which can be biased to test for the effect of secondary electron emission from the

---

[8] R. Mather and E. Segrè, Phys. Rev., in press; (UCRL-1089).

electrodes. The whole Faraday cup structure is in an evacuated enclosure into which the beam passes through a thin window. A magnetic field of 100 gauss across the face of the Faraday cup serves to reduce drastically the secondary electron emission. In operation, change of the bias foil potential from -500 v to +500 v caused only 1/2 percent change in the apparent calibration of the ionization chamber, indicating that secondary electron emission was sufficiently small.

We call the multiplication factor M of the ionization chamber the ratio between the saturation current collected in the chamber and the current in the Faraday cup. We can write

$$M = (t/w)(-dE/dx) \qquad (4)$$

where t is the thickness of the chamber in gr/cm^2 of argon, dE/dx is the specific energy loss in ev gr^{-1} cm^2 and w is the energy in ev spent for producing one ion pair. Assuming at the maximum energy $-dE/dx = 3.08 \times 10^6$ for argon[9] we find that the energy w spent per ion pair produced is 25.5 ev. Assuming this quantity to be independent of energy, and the range energy relations of reference 9 to be correct, we can calculate the multiplication factor of the chamber at the other energies.

The intensity of the beam used varied from 5×10^5 to 5×10^7 protons/sec. The pulses during which the particles come out occupied about one-thousandth of the "beam on" time. The diameter of the beam was usually 1.25 cm. The integrated current in the ionization chamber was measured by passing it into a condenser and measuring the potential across the condenser with an electrometer circuit similar to that of Vance.[10] The leakage resistance of the system was about 10^{13} ohms. When necessary the energy of the

---

[9] Aron, Hoffman, and Williams, AECU-663.

[10] A. W. Vance, Rev. Sci. Inst. 7, 489 (1936).

beam was reduced by inserting lithium absorbers before the collimating channel. Lithium was chosen in order to minimize multiple scattering which lowers the beam intensity. The energy of the protons emerging was then deduced from their range in copper and the tables of Aron, Hoffman, and Williams[9] which were also checked by a direct experiment.[8]

Targets

The targets used were foils of polyethylene $(CH_2)_n$ which weighed 283 mg cm^{-2}. The composition of this substance was kindly checked by the late Dr. Otto Beeck of the Shell Development Company; it was found to contain 14.44 percent hydrogen by weight (theoretical for CH_2 is 14.37). In spite of the coincidence system the coincidence counting rate did not vanish if we replaced CH_2 by carbon of equal stopping power. These residual coincidences were mainly accidentals and their rate could be kept low (1/10) with respect to the main effect by controlling the intensity of the primary beam. In order to subtract them we used a carbon target containing 1.43 times as many carbon atoms per cm^2 as the CH_2 target. This target has approximately the same stopping power for protons as the CH_2 target. Since the way in which the background should be subtracted is not completely unambiguous it is important to keep it small with respect to the main effect.

We calculate H, the effect due to hydrogen, by the formula

$$H = CH_2 - 0.6C - 0.4B \qquad (5)$$

where CH_2, C, and B are the number of counts obtained if the same number of protons crossed the polyethylene target, C target, or no target (blank run). The justification of this formula is as follows: Data from preliminary work show that for 1 single count due to hydrogen there are about 5 single counts due to carbon. On this assumption, taking into account the solid angles subtended by the A and B crystals, we have for one count due to hydrogen in

crystal A when using a CH_2 target

	Crystal A	Crystal B
Counts due to H	1	9
Counts due to C	5	45

Accidental coincidences arise from 5 counts in crystal A and 45 + 8 = 53 counts in crystal B. If we use a carbon target having the same stopping power as the CH_2 target, it must contain 1.43 as much C as the CH_2 target.

We have thus

	Crystal A	Crystal B
Counts due to C	5 x 1.43 = 7	45 x 1.43 = 64

The accidental coincidences in the case of the carbon target are then $7 \times 64 \times \alpha = 448\,\alpha$ where α depends on the instruments used and on the beam intensity. With the CH_2 target we have an accidental coincidence rate given by $5 \times 53 \times \alpha = 265\,\alpha$; $265\,\alpha/(448\,\alpha) = 0.6$. We thus subtract the carbon background by subtracting the carbon effect multiplied by 0.6. It is important that not only the total number of protons be the same but also the current, because C and B are approximately proportional to the current for a constant total number of protons as is to be expected for accidental coincidences. Experimental verification that this procedure is adequate has come from the agreement of cross sections measured over a considerable range of beam intensities.

Geometry

The angle between the protons emerging from the target, which would be 90° in a non-relativistic case is given by:

$$\tan\left(\textcircled{H} + \Phi\right) = \left[(2Mc^2/E) + 1\right] \tan\Phi + (2Mc^2/E) \cot\Phi. \qquad (6)$$

The deviation of $(\textcircled{H} + \Phi)$ from 90° may conveniently be approximated by

$$(\pi/2) - \textcircled{H} - \Phi \simeq (E/4Mc^2) \sin(2\Phi) \qquad (7)$$

where E is the kinetic energy of the incident proton in the lab. system.

The defining crystal A and the larger crystal B are located as in Fig. 1. Given the dimensions and distance of crystal A, which define Ω, the dimensions and distance of B must be so chosen that all p-p scattering processes which register in A register also in B. The condition on the height of crystal B is indicated in Fig. 5 which is a projection in a direction parallel to the beam direction. The analogous condition on the width of crystal B involves the width of crystal A as well as the thickness of the target measured in the direction of crystal A. The size of crystal B must be further increased to allow for the effect of multiple scattering of both emerging protons in the target material. In a typical case the dimensions of A are 1.8 cm high x 3.80 cm wide; of B 3.80 cm high x 2.51 cm wide; the distances TA and TB in projection are 64 cm and 16 cm. The actual distances between the target and the fronts of A and B are 80 cm and 30 cm respectively. In the case described $\Phi = 52.5^\circ$ and $(H) = 32.8^\circ$.

The distance between the target and the crystal which defines the solid angle has been arbitrarily measured from 4 mm inside of the crystal. We do not know exactly how far a particle must penetrate the crystal in order to be counted, but since the total distance between A and T is more than 80 cm, this uncertainty of 2 or 3 mm can not make more than an error of about 0.8 percent in the measurement of the solid angle. A more serious problem is to make sure that the whole front of the crystal is sensitive. The best evidence on the subject is given by the plateaus of the counting rate versus voltage on the photomultiplier, which we have repeatedly checked, and by the fact that several different pairs of crystals in different geometries gave the same cross section within statistics. In a previous paper we reported cross sections obtained with gas counters. They were systematically somewhat higher than the ones obtained with crystal counters.[2] The origin of this discrepancy has been traced to the fact that the brass walls of the

counters were thick (0.3 cm). Protons hitting the brass could, by multiple scattering, be deviated into the gas and thus counted. The order of magnitude of this effect calculated in a crude way was comparable with the disagreement between the gas counter cross sections and the present crystal cross sections. To make certain that our explanation is correct, we put in front of our crystal a brass tube to simulate the geometry of the gas counters. Measurement of the cross sections with this contraption gave again high values in agreement with the gas counter results.

The angle between the target and the beam was chosen in such a way that the plane of the target was tangent to a circle defined by the two crystals and the point where the beam intersects the target. This minimizes the deviations from the optimum geometry for the various points of the target and is essential if crystal A and crystal B are to have approximately the same dimensions.

We checked many times that upon changing the distance between A and T or B and T or both, within the limits prescribed by the geometrical criteria, the cross sections remained unchanged.

Experimental Procedure

A typical run proceeded as follows: The deflected beam of the cyclotron was aligned photographically by replacing the target T and ionization chamber M of Fig. 1 with x-ray films which had fiducial marks accurately located with respect to the scattering table.

After this the plateaus of the coincidence counting rate H versus voltage in the photomultiplier tubes were taken. Results are shown in Fig. 6.

Following this the height of the whole scattering apparatus was changed in small steps and the coincidence counting rate maximized. (Fig. 7.) This guaranteed that the beam, crystal A and crystal B were in a plane. Finally,

keeping (H) constant, Φ was varied to maximize the H count. This last check shows very clearly that the energy of the impinging proton is about 345 Mev (and that the relativistic elastic collision laws are obeyed). (Fig. 8.) The effect vanishes at 90°, indicating that there were few very low energy protons in the beam.

After these tests a measuring run started and we report the numbers obtained in a typical case.

We give as an example the detailed calculation of the eleventh line of Table I. The angle Φ, measured directly is, 52.5°. Knowledge of the incident proton energy allows calculation of the center of mass angle, θ = 70.6° using Eq. (3). (Here we always use whichever angle is less than 90°.) The target thickness if 0.283 gr cm^{-2} of CH_2, and the surface of the target makes an angle of 54.1° with the beam. The number of target atoms per cm^2 along the beam direction is $N = 0.283 \times 2 \times 6.023 \times 10^{23}/(14.03 \times \sin 54.1^\circ) = 3{,}000 \times 10^{22}$ target protons/cm^2. The defining crystal (A) has a face of 1.81 cm x 3.80 cm = 6.88 cm^2, and is located at the effective distance 80.2 cm from the target. The solid angle subtended by the counter, Ω, is then $6.88/(80.2)^2 = 1.070 \times 10^{-3}$ sterad. Crystal B is 3.80 cm high by 2.51 cm wide and is located 30 cm from the target. The ionization chamber for beam monitoring is 5.10 cm deep, and is filled with argon gas to a pressure of 89.6 cm Hg at 22°C (82.9 cm Hg at 0°C). The total capacity in the integration circuit is 1.007×10^{-7} fd.; the integrator circuit is observed to read full scale with 0.993 volts at the input. From these figures and the data obtained in the calibration with the Faraday cup we calculate that $n = 6.86 \times 10^8$ protons for full scale integrator reading ("integrator volt").

The number of counts per integrator volt registered was as follows:

CH_2 : 228 ± 6

C : 52 ± 4

Blank : 26 ± 7;

the time required for one integrator volt was about 100 seconds. From this according to Eq. (5) we obtain

$$H = 187$$

and ε_H (standard deviation) = 8.

We can now calculate the differential scattering cross section in the center of mass system using Eqns. (1) and (2), $\sigma(\theta = 70.6^\circ) = (3.67 \pm 0.16) \times 10^{-27}$ cm^2 sterad^{-1}. Table I and Fig. 10 show all the results obtained at full beam energy with this method.

Small Angles

At small scattering angles the use of polyethylene targets becomes impractical because a coincidence system is hampered by the difficulty of measuring the proton escaping at low energy, and if one abandons the coincidence procedure the scattering by carbon becomes prohibitive. For this reason we decided to use Method I with a liquid hydrogen target and do away with the coincidence method.

The experimental setup is schematically shown in Fig. 9. The liquid hydrogen target was built by Dr. L. J. Cook and will be described by him in another article.[11] The hydrogen containing part of it is a stainless steel tube 34.92 cm long and 5.08 cm diameter closed by two hemispherical foils of stainless steel 0.1 gr/cm^2 thick. Also two identical hemispherical foils form part of the vacuum jacket. The beam, 1.3 cm in diameter, passes through this target hitting only the four terminal hemispheres and the hydrogen but not the side walls. The crystal counters A and B were connected in coincidence and could detect particles from the whole length of the hydrogen target. The measurements proceeded as follows: first, the coincidence counting rate was determined with T full of air, next with T full of liquid hydrogen boiling at atmospheric pressure, and finally the liquid hydrogen was evapor-

[11] To appear soon, probably in the Rev. Sci. Inst.

Table I

Angle θ c.m. system in degrees	Differential cross section $\sigma(\theta)$ in $10^{-27}cm^2$/sterad.	Error in $\sigma(\theta)$ in $10^{-27}cm^2$/sterad.	E lab. system in Mev
35.6	4.31	0.21	345
36.4	3.93	0.15	"
43.4	3.79	0.15	"
44.0	4.17	0.13	"
45.8	3.64	0.07	"
46.1	3.99	0.11	"
52.4	3.77	0.10	"
60.8	3.83	0.13	"
64.0	3.55	0.11	"
64.0	3.74	0.14	"
70.6	3.67	0.16	"
72.2	3.67	0.11	"
80.2	3.95	0.12	"
87.6	3.86	0.10	"
88.2	3.91	0.08	"
88.2	3.70	0.08	"
88.6	3.85	0.06	"
88.6	3.54	0.09	"
89.2	4.15	0.36	"

ated and the background redetermined. This cycle was repeated twice. The angle Φ was varied from 5 to 25 degrees in order to overlap with measurements obtained by the coincidence system. The results are contained in Table II. It will be noted that the consistency of the data is good, but there is a deviation of about 10 percent between these data and those obtained with the coincidence system. More work on this point would clearly be desirable, because the discrepancy is not yet accounted for.

Table II

Liquid H_2 Run

Angle θ c.m. system in degrees	Differential cross section $\sigma(\theta)$ in $10^{-27}cm^2$/sterad.	Error in $\sigma(\theta)$ in $10^{-27}cm^2$/sterad.	E lab. system in Mev
11.3	5.1	0.36	345
11.3	5.38	0.49	
15.2	3.71	0.22	
15.2	3.21	0.17	
21.1	3.51	0.10	
21.7	3.06	0.15	
32.5	3.52	0.09	
33.1	3.51	0.11	
42.8	3.48	0.10	
42.8	3.40	0.08	
53.2	3.40	0.08	
53.2	3.28	0.10	

Lower Energies

Results at reduced energies are reported in Table III, and the differential cross sections at 90° (c.m.) are shown in Fig. 11. Only the coincidence

Table III

Angle θ c.m. system in degrees	Differential cross section $\sigma(\theta)$ in $10^{-27}cm^2$/sterad.	Error in $\sigma(\theta)$ in $10^{-27}cm^2$/sterad.	E lab. system in Mev
47.4	3.97	0.51	250
47.4	3.23	0.29	250
62.0	4.38	0.27	247
64.6	3.84	0.20	250
78.4	3.69	0.15	250
78.4	3.53	0.18	250
87.2	3.67	0.21	250
87.4	3.69	0.10	249
87.6	3.95	0.22	250
87.6	3.59	0.21	250
89.6	3.56	0.27	247
89.6	3.28	0.16	247
59.9	3.38	0.23	164
60.8	4.08	0.45	163
88.6	3.88	0.26	163
88.8	3.54	0.35	164
90.0	3.60	0.17	164
63.0	3.67	0.56	120
63.0	4.40	0.50	120
77.8	4.25	0.33	120
85.2	3.85	0.25	120
89.2	3.95	0.12	118

method (method II) has been used at reduced energies. The beam is greatly attenuated (to 1/100 normal intensity) by multiple scattering in the lithium and the beam loses its parallelism so the only effective collimation is by the 48-inch long collimating tube shown in Fig. 3. The effect of previous collimating slits is reduced drastically by the multiple scattering. Therefore, the beam is more spread and more divergent than the full energy beam and larger crystals of stilbene have been necessary to obtain satisfactory geometry. Relative to the proton beam intensity the background is considerably increased, presumably due to neutrons formed in the lithium and in

the brass of the collimator.

Precision of the Results

The errors quoted in Table I are standard deviations due to statistics only. In addition to these we have to consider errors in the various quantities H, N, n, Ω, and Φ which enter in the expression for $\sigma(\theta)$. For the target: area, mass, uniformity, composition. These all together may make 1 percent. The effective thickness of the target depends on the angle δ of Fig. 1. The imprecision of the adjustment of this angle may make another 1 percent error.

The measurement of H is affected by statistical errors and by the uncertainty inherent in the background subtraction method. The measurement of the solid angle of the crystals is affected by the precision of the geometrical measurements which is good (1.5 percent) but is subject to the assumption that all the crystal is sensitive. This in turn is proved by the plateaus of the coincidence counting rate versus voltage. The error introduced here is hard to estimate and is probably one of the weakest points of this investigation. We give as an estimate 3 percent error. Some reassurance on this point was obtained by using various sets of crystals and distances. The cross section obtained were identical within the statistical accuracy of the measurements.

Multiple scattering in the target and in the crystals is negligible, since crystal B was in all cases sufficiently larger than dictated by geometical considerations alone.

The measurement of the current in the primary beam is subject to the uncertainty of the electrical apparatus, saturation of the current in the ionization chamber, and calibration with the Faraday cup. Two percent error may be a fair estimate for this part of the measurement.

All together the imprecision may be estimated to be the counting errors

shown in Table I superimposed on a 5 percent error due to other factors. The points obtained are each independent of the others and represent absolute measurements. The agreement between them gives a fair idea of the overall consistency of the experiment.

Analysis of the liquid hydrogen results of Table II indicate that they too should be given a 5-percent error superimposed on the counting error shown in the table. Reduced energy results (Table III) are subject to greater uncertainties, amounting to about 7-percent error superimposed on those of the table.

Interpretation

A maximum program for the interpretation of n-p and p-p scattering experiments would be to deduce the cross section from meson theory. At the present stage of the theory this is clearly impossible and we must be content with more modest procedures.

The attempt has been made by many people to interpret the scattering experiments with velocity independent forces.[12] Accepting the usual symmetry restrictions one is left, for particles of spin 1/2, with a fairly broad class of potentials:

$$V = V_1 + \underline{\sigma}_1 \cdot \underline{\sigma}_2 V_2 + S_{12} V_3 \qquad (8)$$

where V_1, V_2 and V_3 are functions of the separation distance and may be different for even and odd quantum numbers of the orbital angular momentum. $\underline{\sigma}_1$ and $\underline{\sigma}_2$ are the spin operators and S_{12} is the tensor force operator. These attempts have been reasonably successful in several cases in explaining high energy scattering with potentials which also show proper agreement with the

[12] A partial list includes M. Camac and H. A. Bethe, Phys. Rev. 73, 191 (1948); T. Wu, Phys. Rev. 73, 934 (1948); J. Ashkin and T. Wu, Phys. Rev. 73, 973 (1948); Massey, Burhop, and Hu, Phys. Rev. 73, 1403 (1948); Burhop and Yadav, Proc. Roy. Soc. A197, 505 (1949); R. S. Christian and E. W. Hart, Phys. Rev. 77, 441 (1950); R. S. Christian and H. P. Noyes, Phys. Rev. 79, 85 (1950); Robert Jastrow, Phys. Rev. 79, 389 (1950).

low energy properties of the n-p or p-p system respectively. As an example of these attempts we report the results of calculations by Christian and Hart for the n-p scattering in Fig. 12.

It will be noticed that whereas the form of the curves fits reasonably well, the calculated cross sections are in all cases higher than the observed cross sections.[1, 13] The theoretical curves are to be considered the best fits in this case, for the angular distributions are thought to be better known than the total cross sections. For instance, at 90 Mev the angular distribution is probably known to about 5 percent while the total cross section is known only to 15 percent. (The uncertainties in the total cross sections stem not from the cross section measurements themselves, but from the uncertainties in the effective energies at which the observed cross sections should be considered to apply.) Nevertheless there is a fairly clear discrepancy between calculated and observed cross sections for n-p scattering at 90 Mev, for the experiments indicate that the product $E\sigma_t$ is definitely less than 8×10^{-24} Mev-cm^2, while the calculated value of Christian and Hart is 9.3×10^{-24} Mev-cm^2.

For the p-p scattering we show in Fig. 13 the results of Christian and Noyes. The parameters have been changed for us by Swanson, to give the best fit to the present results. The forces used here differ from those used in the n-p calculations of Fig. 12 mainly in the addition of a strong odd-wave tensor force with a singularity at the origin. Within this framework no way has been found to remove the large discrepancy between observed and calculated cross sections near 15°, 345 Mev. Omission of the tensor part of the force would create an insurmountable difficulty inasmuch as it would produce a vanishingly small cross section at 90°.

---

[13] Cook, McMillan, Peterson, and Sewell, Phys. Rev. 75, 7 (1949); J. DeJuren and N. Knable, Phys. Rev. 77, 606 (1950).

In view of the strong arguments from low energy phenomena favoring the identity of the n-n and p-p forces it is very tempting to extend this result and try the hypothesis of the identity of the n-p, p-p, and n-n interactions. Qualitative support for this hypothesis has recently been given by Jastrow. The low energy n-p and p-p scattering experiments do not conflict with this viewpoint. The large apparent differences between high energy n-p and p-p scattering cross sections do not rule out this possibility because the Pauli principle eliminates half of the states (triplet s, singlet p, etc.) from p-p or n-n scattering. The absence of half of the states in the case of systems with identical particles gives a large leeway in the choice of potentials to fit both problems.

Actually the most that we can hope to do with the semiempirical line of approach followed is to exhibit a special potential compatible with all the experimental material available including high energy p-p and n-p scattering.

It might be possible, however, to do the opposite, namely to prove that the potentials are different. The only simple theorem now known to us is the following: If the n-p and p-p potentials are the same and if there are no tensor forces, then

$$\sigma_{p-p}\,(\theta = 90^{\circ}) \leq 4\,\sigma_{n-p}\,(\theta = 90^{\circ}). \qquad (9)$$

Unfortunately, we know of no such limitation for cases in which tensor forces are allowed. Furthermore even this relationship is not violated as far as it is now known. The case which comes closest to violation of the above rule is that at 260 Mev, where the p-p differential cross section is $(3.6 \pm 0.2) \times 10^{-27}$ cm^2/sterad., and the corresponding n-p cross section is $(1.3 \pm 0.2) \times 10^{-27}$ cm^2/sterad. The ratio is 2.8 ± 0.5, so the rule (limited as it is) is not broken.

It remains, then, to try to show at least one potential which corresponds to both p-p and n-p scattering. We mention three cases of interest

with which we have the greatest familiarity. First, the Christian and Hart potential for the n-p scattering used in Fig. 12 gives for the p-p scattering negligible intensity in the range of angles 50° to 90° and so disagrees with the p-p experiments.

Secondly, the Christian and Noyes potential developed for p-p scattering may be applied to the n-p scattering. Fig. 14 shows the cross sections for n-p scattering, as calculated for us by Swanson with experimental points, using the same potential as in the p-p case of Fig. 13. The agreement is not excellent, but the qualitative features are reasonably well represented. The calculations have been made using Born approximation in odd states, but a more exact method has been used in even states. The unexpected behavior near 30° may be the result of the approximation used. The calculated total cross section is as usual too high. These curves are included here because they give a better fit to the n-p experiments than was at first supposed, and for comparison with the calculations of Jastrow.

The third case of interest is that of Jastrow,[12] who chooses a potential with a strong repulsion at short distances. The same potential has been used to calculate both n-p and p-p scattering. His results, along with experimental points, are shown in Figs. 15 and 16. He has kindly extended his calculations for us to include in the angular distribution the effect of tensor forces in odd states. The calculations were made using Born approximation except in the case of the s-wave, where a more exact method has been used. The n-p curve of Fig. 16 shows unexpected maxima near 30° and 130° which are thought to be peculiar to the approximation used.

In Jastrow's results, as in those of Christian and Noyes, a large discrepancy appears in the p-p scattering at 15°, 345 Mev. Coulomb effects have not been included in the calculation. However the coulomb effect, even in the form of interference with the specifically nuclear scattering,

cannot account for more than a small part of the discrepancy at 15°. The n-p results (Fig. 16) are remarkably good, but the calculated total cross section is still slightly too high. All together one can say that these attempts are only moderately successful.

If we abandon the restriction to velocity independent forces, then the variety of choices becomes practically unlimited. One of the simple possibilities is to introduce a spin orbit coupling for which there are also independent indications in the nuclear shell structure. This has been done by Case and Pais[14] and they also conclude that with this generalized form of interaction it may be possible to preserve the identity between n-p and p-p forces, although we do not know the quantitative results of their calculations.

In all these calculations relativity has not been taken into account. The changes brought about by relativity are guessed to be of the order of 0.2 of the cross sections.

In conclusion we must rather disappointingly admit that all the evidence accumulated on n-p and p-p scattering at high energy does not yet allow a sure answer to the question of the charge independence of nuclear forces.

Acknowledgments

Through the Radiation Laboratory this work has been supported by the United States Atomic Energy Commission.

The authors are grateful to the cyclotron operating crew for their lasting patience and to Dr. V. Z. Peterson for his helpfulness with both the liquid hydrogen target and the Faraday cup.

---

[14] K. M. Case and A. Pais, Phys. Rev. 80, 203 (1950).

Figure Captions

Fig. 1. Arrangement of the coincidence apparatus, top view. The angles used in the test are shown on this figure.

Fig. 2. Schematic diagram of the cyclotron, deflecting magnet, and collimator.

Fig. 3. Collimator for the proton beam. In this figure we also show the lithium absorbers occasionally used to reduce the energy of the beam. The mechanism for moving the collimator hole is not shown.

Fig. 4. Detail of the monitoring ionization chamber and of the Faraday cup as assembled for calibration of the ionization chamber.

Fig. 5. Relative size and position of defining and coincident crystal viewed from the direction of the beam. The two crystals and the beam are shown on scale. The separation distances of each crystal from the beam are reduced to 1/2 that scale.

Fig. 6. Voltage plateau. Abscissa: voltage on the photomultipliers connected with crystals A and B. Ordinate: number of coincidences due to hydrogen for a fixed number of protons crossing the target. (The figure shows the coincidence counting rate at the average beam level used.)

Fig. 7. Number of coincidences due to CH_2 for a fixed number of protons crossing the target versus height of the plane containing crystals AB and the target. This plane is initially parallel to the beam and is adjusted to contain the beam by lifting the whole apparatus.

Fig. 8. Coincidence counting rate as a function of the angle $(\textcircled{H} + \Phi)$ between the two crystals for $\textcircled{H} = 43^\circ$. According to Eq. (6) a maximum at 84.7° corresponds to E = 345 Mev.

Fig. 9. Vertical section of the liquid hydrogen apparatus for measuring scattering at small angles to the beam. The counter arm pivots

around an axis through the center of the liquid hydrogen container. Not shown is a thin heat shield which surrounds the liquid hydrogen container and is maintained at liquid nitrogen temperature.

Fig. 10. Differential scattering cross section in center of mass coordinate system, $\sigma(\theta)$. The errors shown are standard deviations from counting statistics only. Circles: CH_2 target, coincidence method (method II). Crosses: liquid hydrogen, single counter (method I). Square: CH_2 target, single counter (method I).

Fig. 11. Differential scattering cross section for $\theta = 90^\circ$ as a function of energy, in 10^{-27} cm^2/steradian. Errors indicated are standard deviations from counting statistics only.

Fig. 12. The curves show the calculated differential cross sections of Christian and Hart. The points are experimental values, taken from the papers of reference 1, except the large X which was obtained from private communication from Dr. Robert H. Fox. The experimental total cross sections might be in error by as much as 20 percent, as would be needed to give good fit. In the calculations Christian and Hart used the following potential: For singlet states $V = (-35.3$ Mev$) \left[(1/2) + (1/2)\ P_x\right] (r_o/r) \exp(-r/r_o)$; for triplet states $V =$ (-25.3 Mev$) \left[(1/2) + (1/2)\ P_x\right] (r_o/r) \exp(-r/r_o) +$ (-48.2 Mev$) (0.37 + 0.63\ P_x) (r_o/r) \exp(-r/r_o)\ S_{12}$, where S_{12} is the tensor force operator and $r_o = 1.35 \times 10^{-13}$ cm in all cases. P_x is the space exchange operator.

Fig. 13. Points represent experimental results, 345 Mev. Curves are those calculated by Swanson using the method of Christian and Noyes. In the calculations the following potentials were used: For singlet states $V =$ (-13.273 Mev$) (1/2 + (1/2)\ P_x)$ for $r < r_1$ and $V = 0$ for $r > r_1$; for triplet states $V =$ (-25.3 Mev$) (1/2 + (1/2)\ P_x) (r_2/r)$

$\exp(-r/r_2) + (-48.3\ \text{Mev})\ (1/2 + (1/2)\ P_x)\ (r_2/r) \exp(-r/r_2)\ S_{12} + (-15.25\ \text{Mev})\ (1/2 - (1/2)\ P_x)\ (r_3/r)^2 \exp(-r/r_3)\ S_{12}$. $r_1 = 2.615 \times 10^{-13}$ cm, $r_2 = 1.35 \times 10^{-13}$ cm, and $r_3 = 1.6 \times 10^{-13}$ cm.

Fig. 14. n-p scattering calculated with the same potential used for p-p scattering in Fig. 13.

Fig. 15. Experimental points and curves as calculated by Jastrow using the following potential: In singlet states $V = \infty$ when $r < r_o$, $V = (-375\ \text{Mev}) \left[(1/2) + (1/2)\ P_x\right] \exp\left[-(r - r_o)/r_s\right]$ when $r > r_o$ where $r_o = 0.60 \times 10^{-13}$ cm, $r_s = 0.40 \times 10^{-13}$ cm; in triplet states $V = (-69\ \text{Mev}) \left[(1/2) + (1/2)\ P_x + (0.3 + 0.7\ P_x) \times 1.84\ S_{12}\right] \exp(-r/r_t)$ where $r_t = 0.75 \times 10^{13}$ cm.

Fig. 16. Experimental points and curves as calculated by Jastrow using the potential given in Fig. 15.

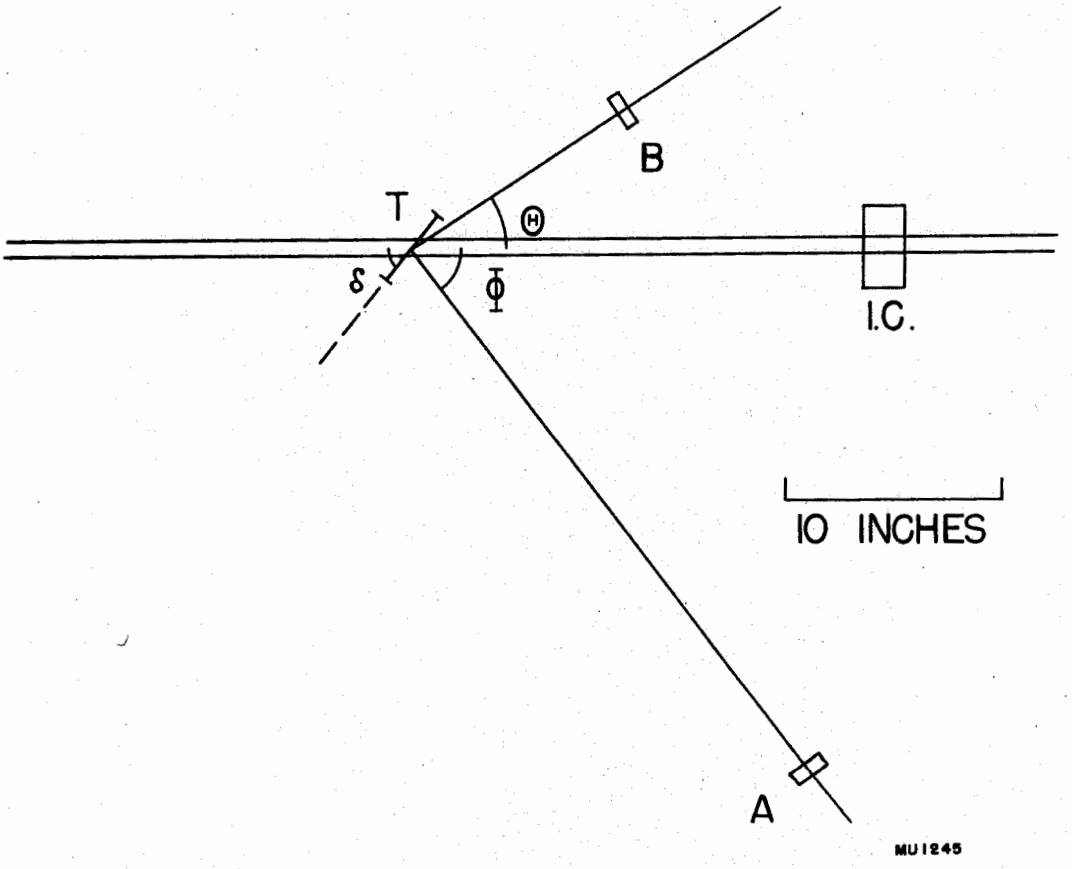

Fig. 1

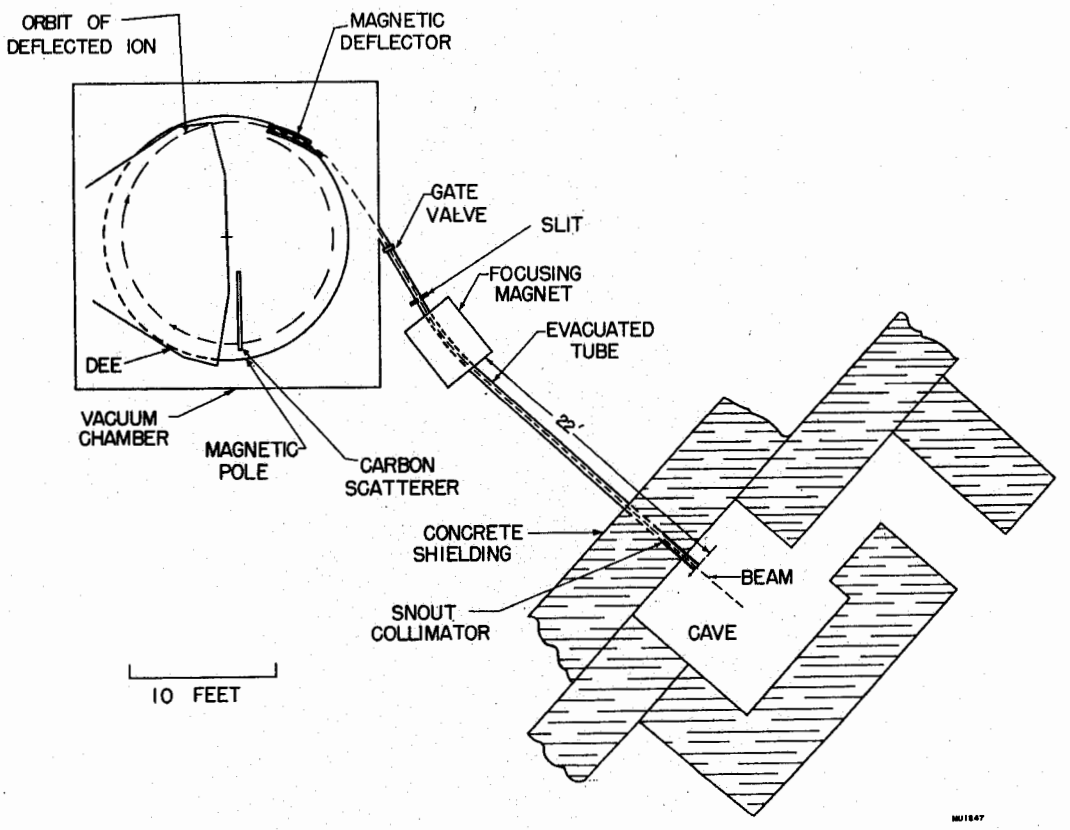
ORBIT OF
DEFLECTED ION
MAGNETIC
DEFLECTOR
GATE
VALVE
SLIT
FOCUSING
MAGNET
EVACUATED
TUBE
DEE
VACUUM
CHAMBER
MAGNETIC
POLE
CARBON
SCATTERER
22'
CONCRETE
SHIELDING
BEAM
SNOUT
COLLIMATOR
CAVE
10 FEET

Fig. 2

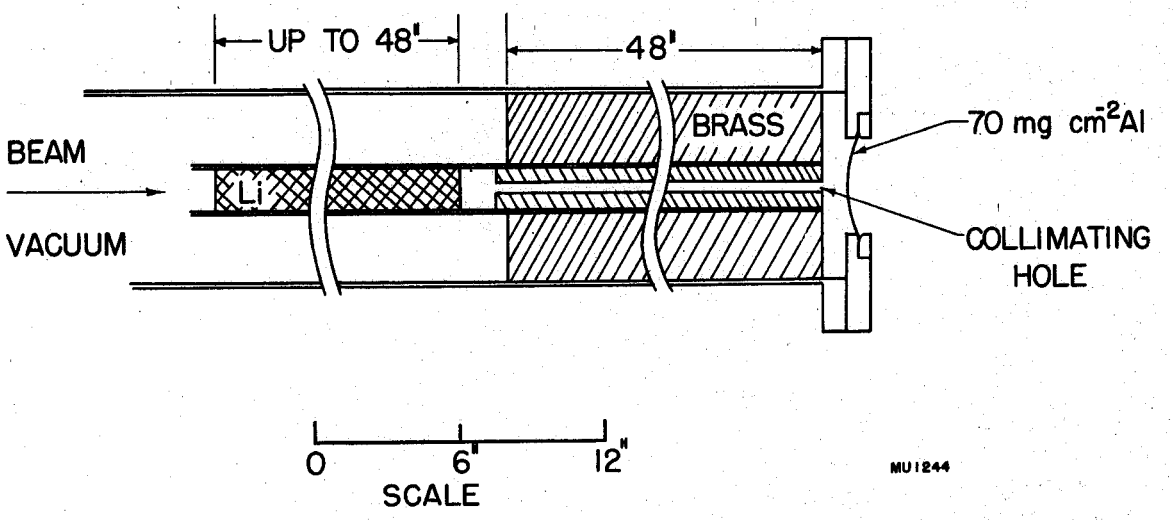
UP TO 48"
48"
BRASS
70 mg cm⁻² Al
BEAM
Li
VACUUM
COLLIMATING HOLE
0
6"
12"
SCALE
MU1244

Fig. 3

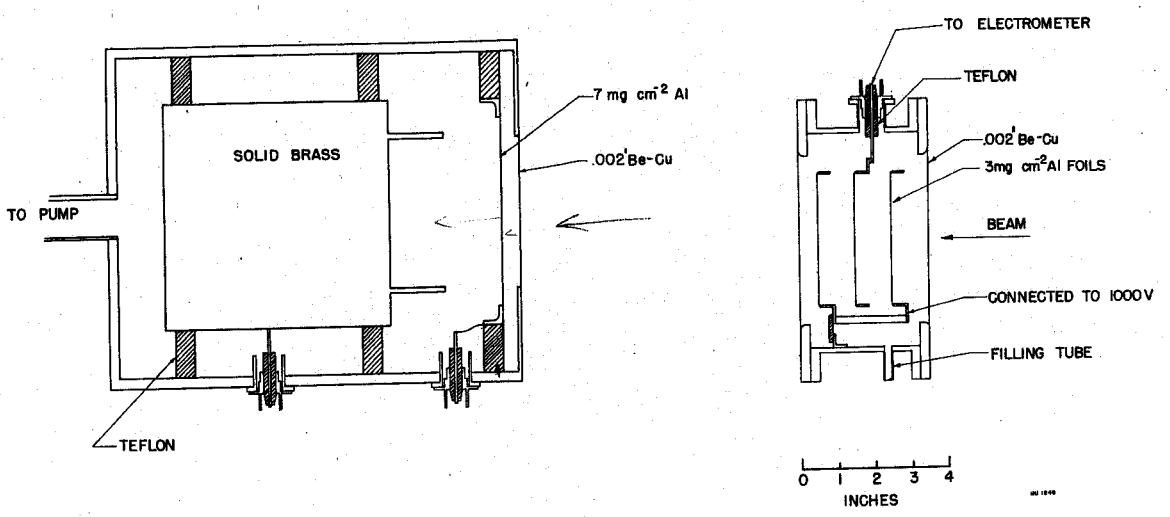
SOLID BRASS
7 mg cm⁻² Al
.002' Be-Cu
TO PUMP
TEFLON
TO ELECTROMETER
TEFLON
.002' Be-Cu
3mg cm⁻² Al FOILS
BEAM
CONNECTED TO 1000V
FILLING TUBE
0 1 2 3 4
INCHES

Fig. 4

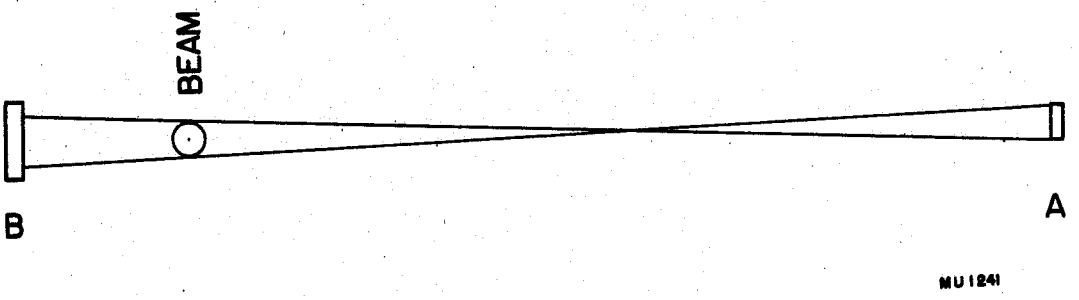

Fig. 5

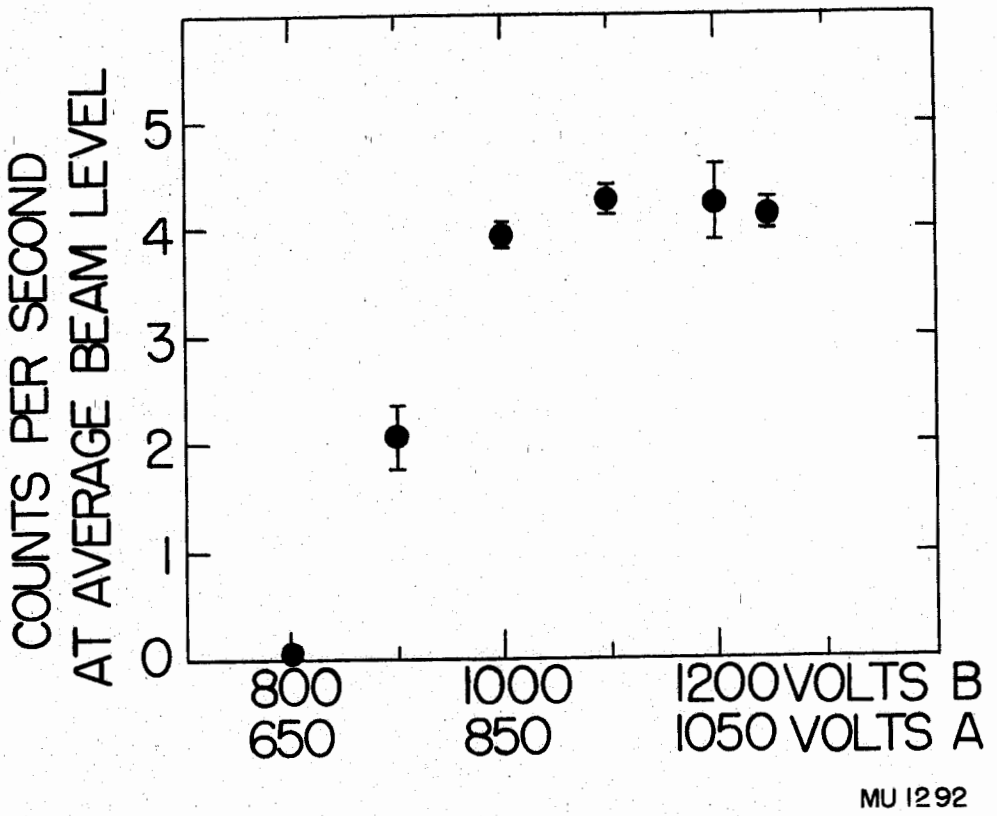
COUNTS PER SECOND
AT AVERAGE BEAM LEVEL
0
1
2
3
4
5
800
650
1000
850
1200 VOLTS B
1050 VOLTS A
MU 1292

Fig. 6

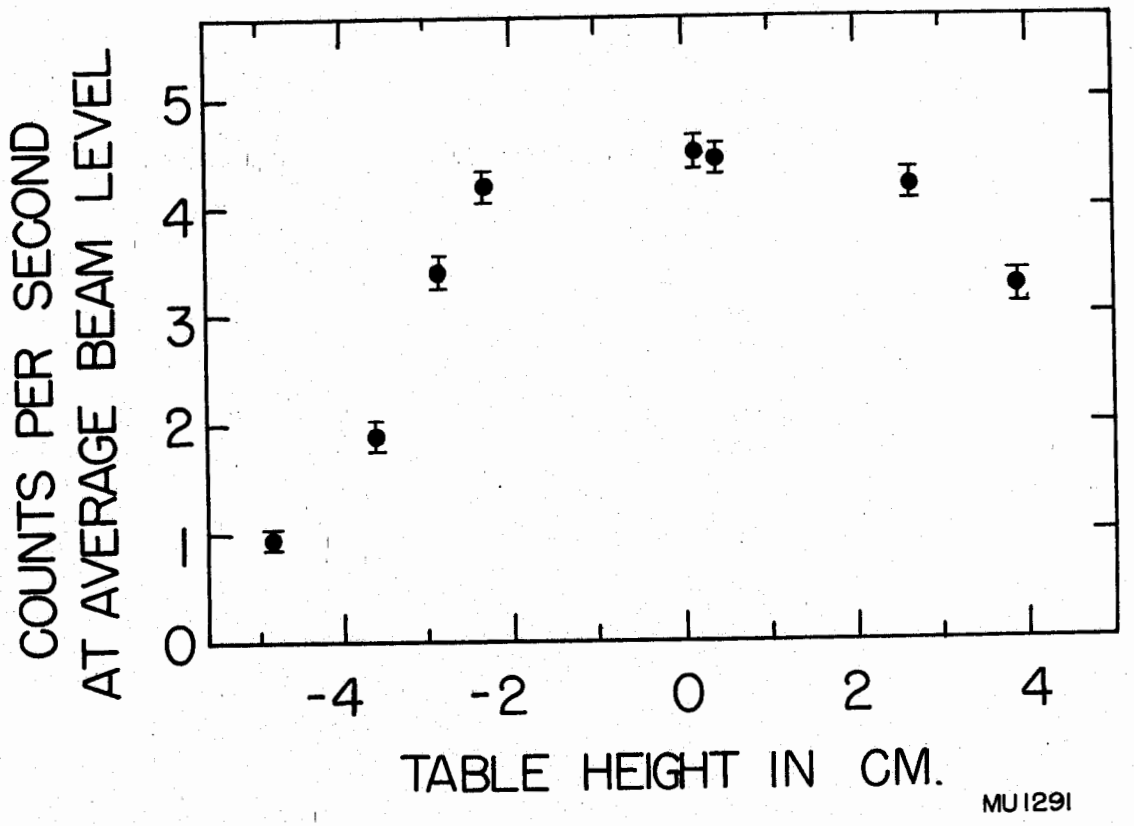
COUNTS PER SECOND
AT AVERAGE BEAM LEVEL
0
1
2
3
4
5
-4
-2
0
2
4
TABLE HEIGHT IN CM.
MU1291

Fig. 7

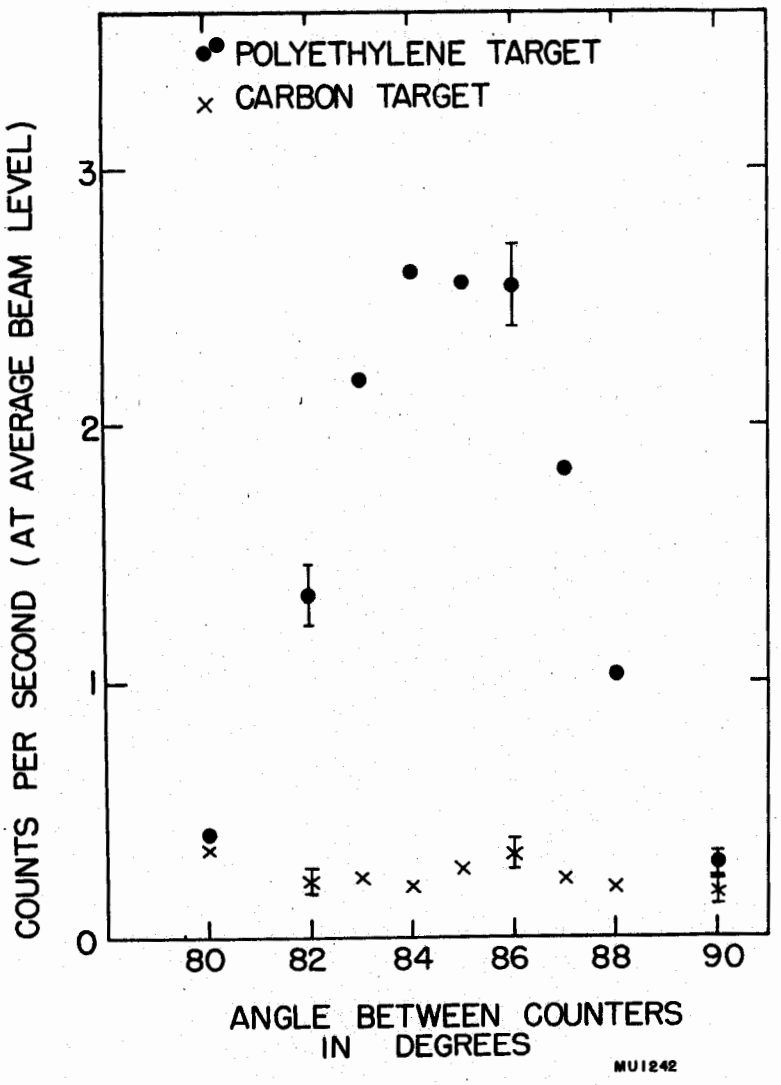
POLYETHYLENE TARGET
CARBON TARGET
COUNTS PER SECOND (AT AVERAGE BEAM LEVEL)
0
1
2
3
80
82
84
86
88
90
ANGLE BETWEEN COUNTERS IN DEGREES
MU1242

Fig. 8

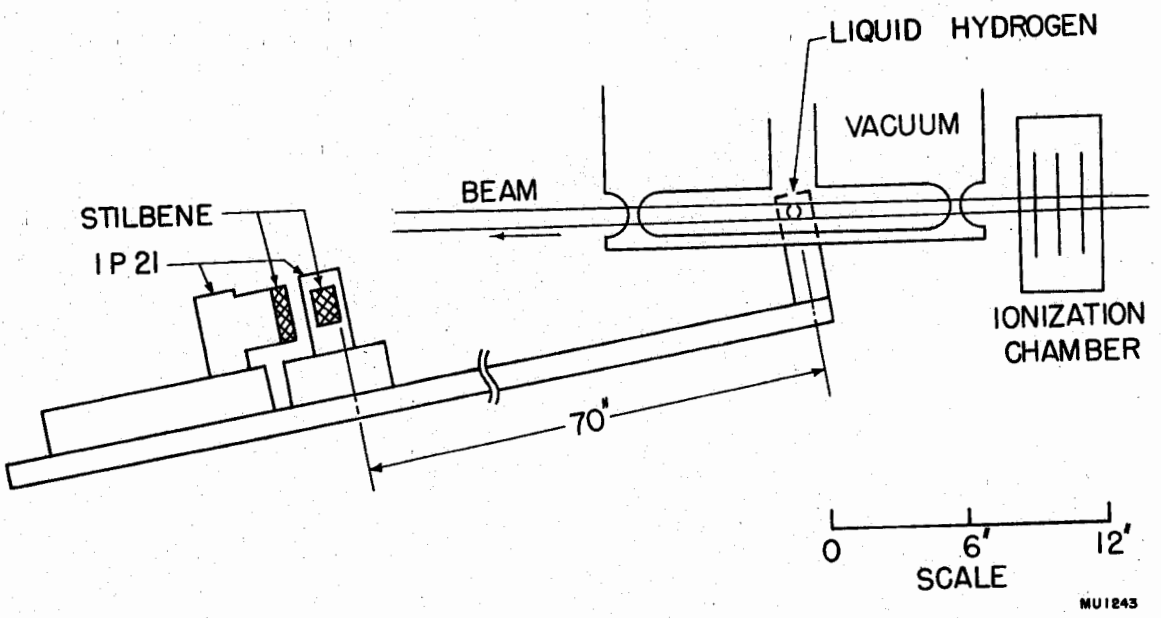
LIQUID HYDROGEN
VACUUM
BEAM
STILBENE
IP 21
IONIZATION
CHAMBER
70"
0
6"
12"
SCALE
MU1243

Fig. 9

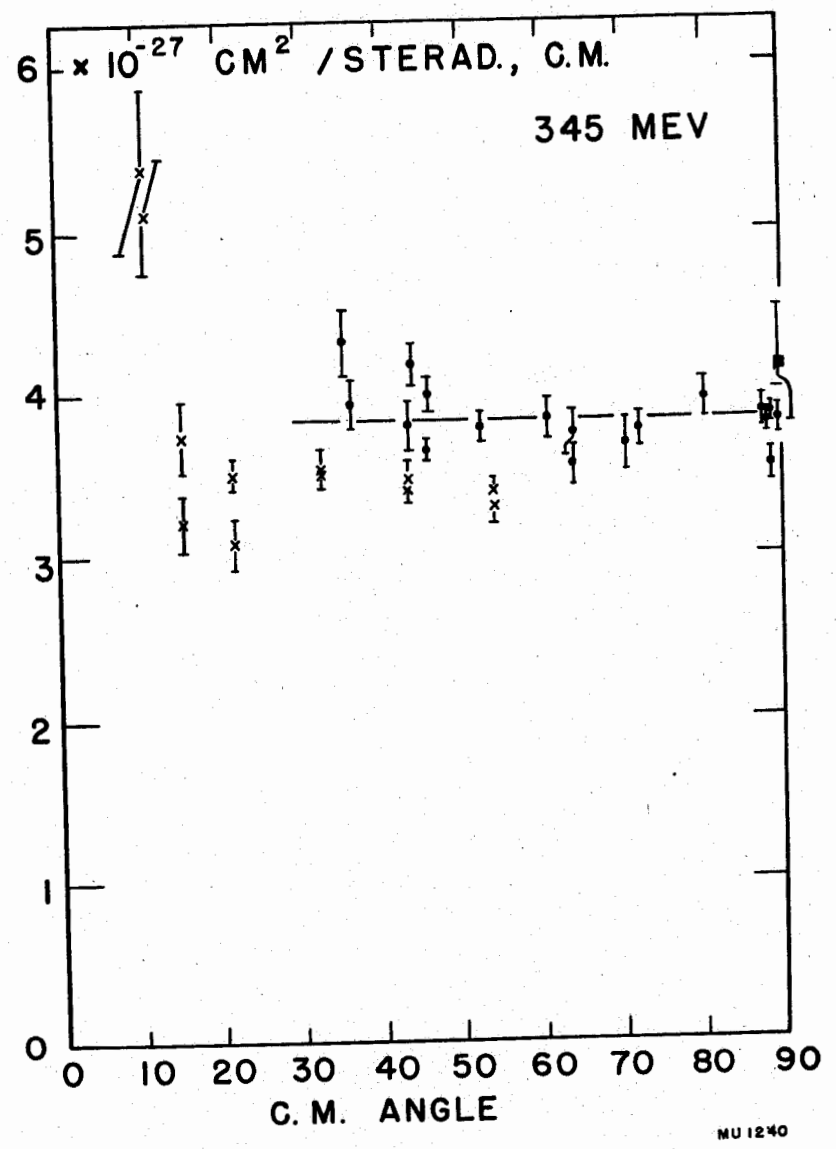
× 10^-27 CM^2 / STERAD., C.M.
345 MEV
6
5
4
3
2
1
0
0 10 20 30 40 50 60 70 80 90
C. M. ANGLE
MU 1240

Fig. 10

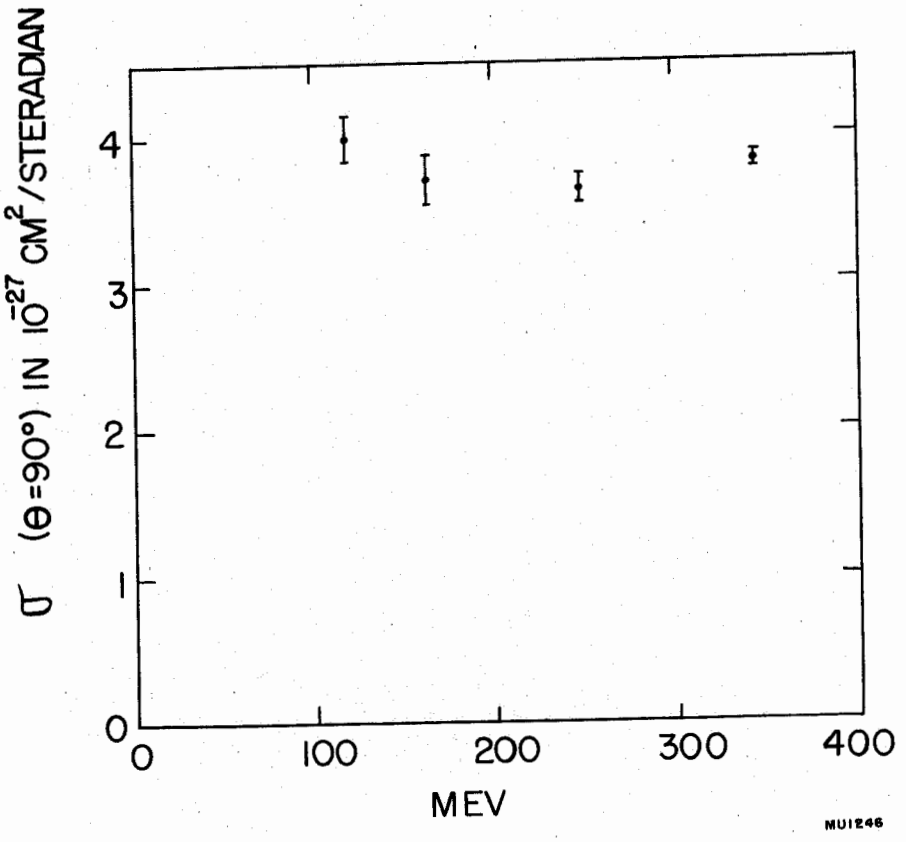

Fig. 11

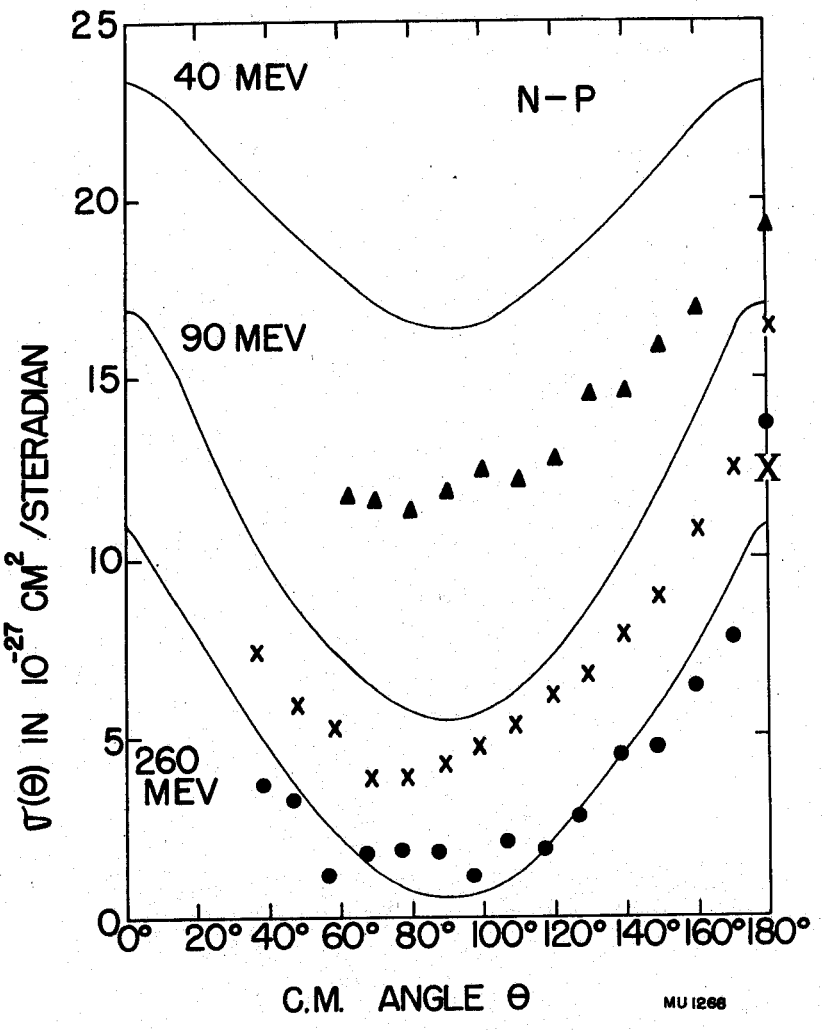
25
20
15
10
5
0
40 MEV
N-P
90 MEV
260
MEV
σ(θ) IN 10^-27 CM^2 /STERADIAN
0° 20° 40° 60° 80° 100° 120° 140° 160° 180°
C.M. ANGLE θ
MU 1268

Fig. 12

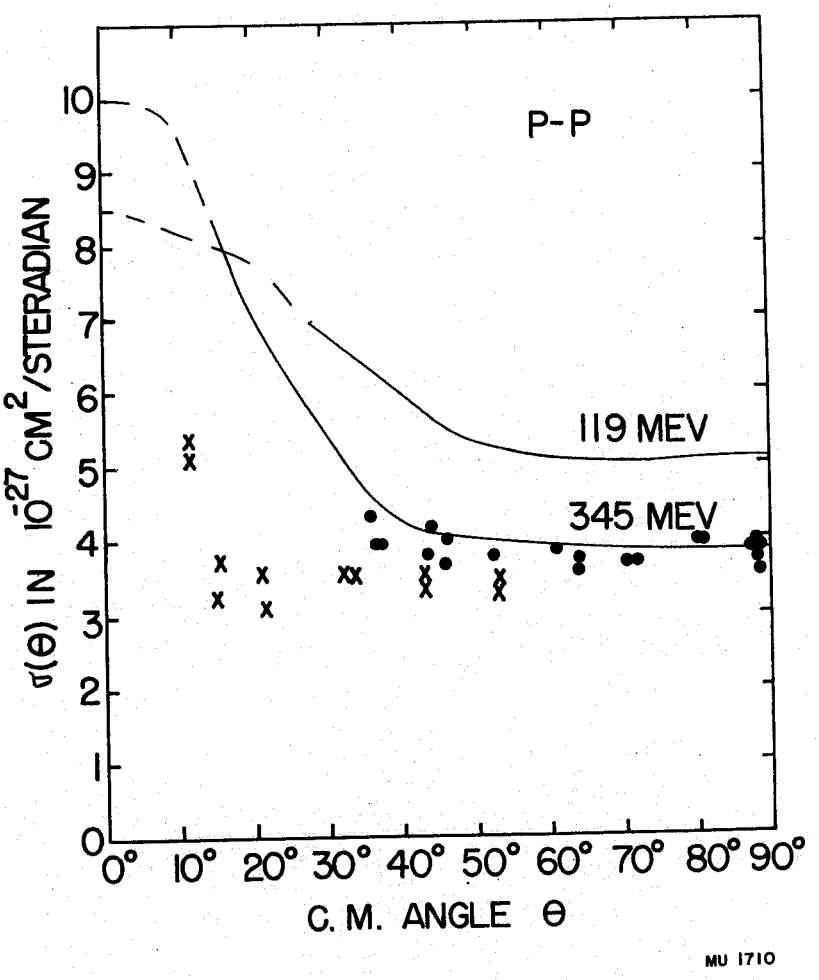
P-P
119 MEV
345 MEV
σ(θ) IN 10^-27 CM^2/STERADIAN
C. M. ANGLE θ
0° 10° 20° 30° 40° 50° 60° 70° 80° 90°
0 1 2 3 4 5 6 7 8 9 10
MU 1710

Fig. 13

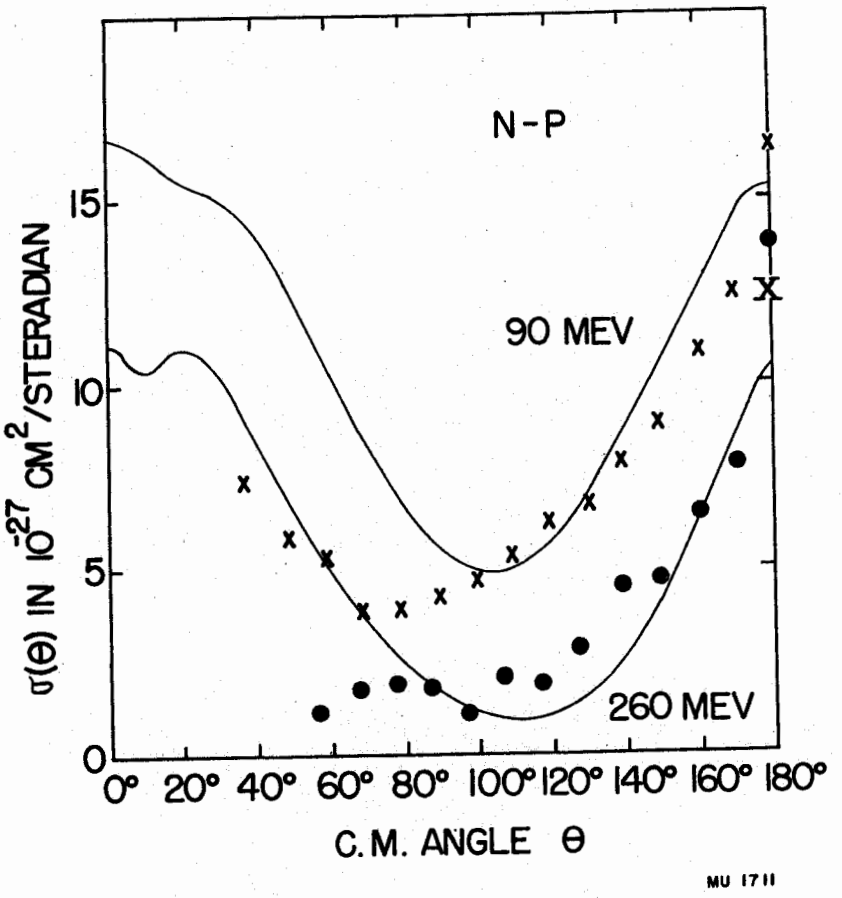
N-P
90 MEV
260 MEV
σ(θ) IN 10^{-27} CM^2/STERADIAN
0
5
10
15
0° 20° 40° 60° 80° 100° 120° 140° 160° 180°
C.M. ANGLE θ
MU 1711

Fig. 14

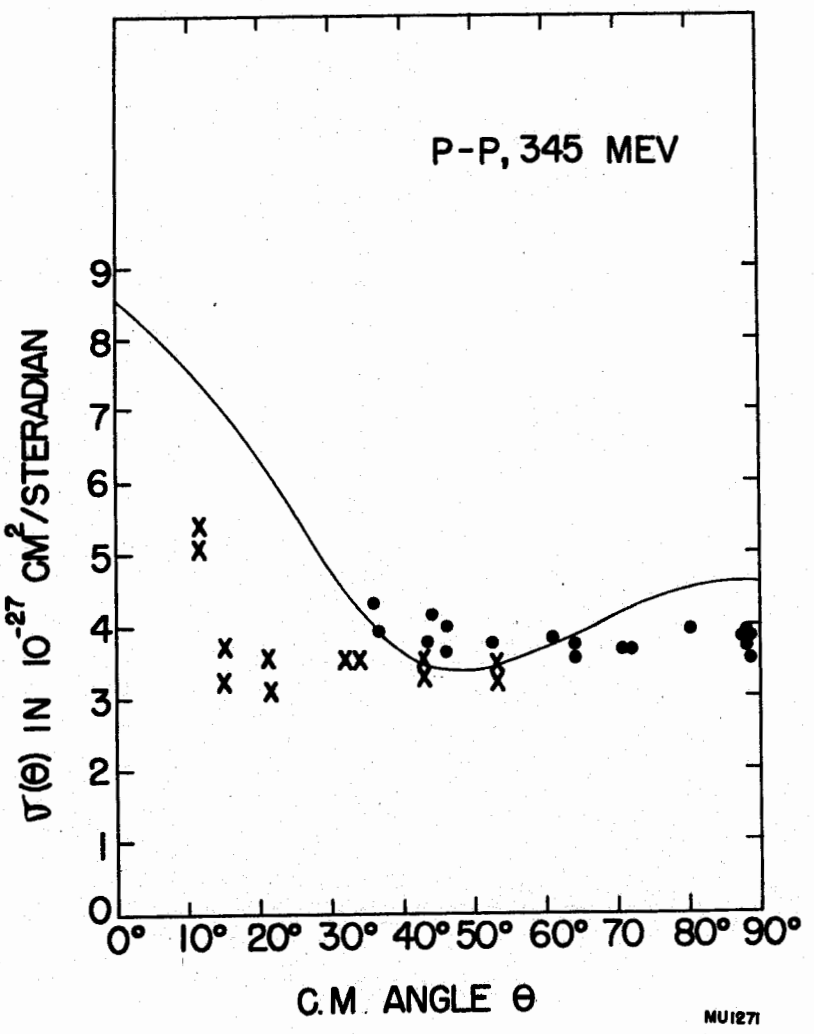
P-P, 345 MEV
σ(θ) IN 10^-27 CM^2/STERADIAN
0
1
2
3
4
5
6
7
8
9
0° 10° 20° 30° 40° 50° 60° 70 80° 90°
C.M. ANGLE θ
MU1271

Fig. 15

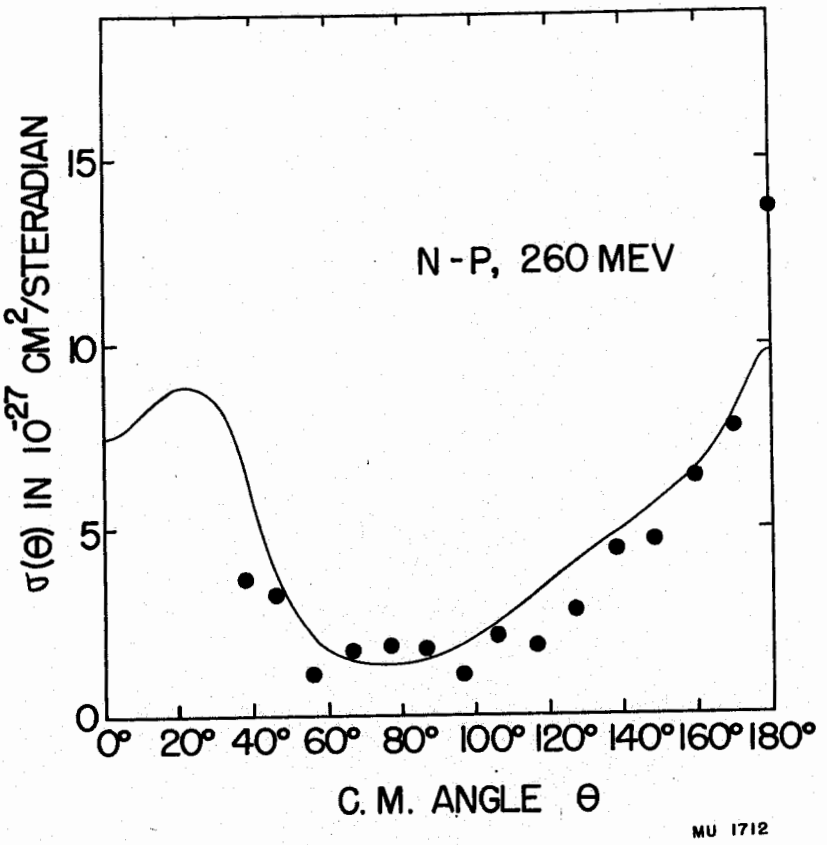
N - P, 260 MEV
σ(θ) IN 10^-27 CM^2/STERADIAN
0
5
10
15
0° 20° 40° 60° 80° 100° 120° 140° 160° 180°
C. M. ANGLE θ
MU 1712

Fig. 16